X-672-74-226

PREPRINT

NASA TM X- 70727

TWO HIGH RESOLUTION VELOCITY VECTOR ANALYZERS FOR COSMIC DUST PARTICLES

AUGUST 1974

GSFC

GODDARD SPACE FLIGHT CENTER

GREENBELT, MARYLAND

X-672-74-226

TWO HIGH RESOLUTION VELOCITY VECTOR ANALYZERS FOR COSMIC DUST PARTICLES

Siegfried Auer
Laboratory for Optical Astronomy

August 1974

GODDARD SPACE FLIGHT CENTER
Greenbelt, Maryland 20771

TWO HIGH RESOLUTION VELOCITY VECTOR ANALYZERS FOR COSMIC DUST PARTICLES

Siegfried Auer
Laboratory for Optical Astronomy

ABSTRACT

Two new methods are described to measure velocities and angles of incidence of charged cosmic dust particles with precisions of about 1 percent and 1 degree, respectively. Both methods employ four one-dimensional position-sensitive detectors in series. The first method utilizes a charge-dividing technique while the second utilizes a time-of-flight technique for determining the position of a particle inside the instrument. The velocity vectors are measured although mechanical interaction between the particle and the instrument is completely avoided. Applications to cosmic dust composition and collection experiments are discussed. The range of radii of measurable particles is from about 0.01 to 100 μm at velocities from 1 to 80 km/s.

CONTENTS

ILLUSTRATIONS

TABLES

TWO HIGH RESOLUTION VELOCITY VECTOR ANALYZERS FOR COSMIC DUST PARTICLES

INTRODUCTION

Results from cosmic dust experiments in deep space (Pioneer 8 and 9)[1] and on the lunar surface (Apollo 17) indicate that cosmic dust particles are found in elliptic orbits around the sun as well as in hyperbolic orbits. One particle was definitely observed to have a hyperbolic orbit which could only have come from interstellar space.[2] Interstellar origin of a few other particles is still possible, but not certain at the present time due to large uncertainties in the measured orbital parameters of these dust particles. Pioneer 8 and 9 cosmic dust data show a strong evidence that many hyperbolic dust particles are formed within 1 a.u. from the sun and moving essentially radially away from the sun.[3] They may have been generated by inter-particle collisions in the vicinity of the sun;[4] or they may have been ejected from the solar atmosphere.[5] This question, although of great astrophysical importance, still remains unanswered. An instrument with a high resolution in both angle and velocity measurements would help greatly in answering not only the above questions, but also in studying peculiar motions of interstellar dust particles and in determining the parallactic motion of the sun with respect to the local interstellar dust environment. Also such an instrument would enhance our knowledge on the orbital correlations between the dust particles and their parent bodies, such as comets, asteroids, and possibly the moon. This paper describes two new position-sensitive detectors,

each of which can be used to build an instrument with an angular resolution of about 1 degree and a velocity resolution of about 1 percent. Furthermore, both detectors have the advantage that they perform measurements without touching the particle mechanically. In that way, it will be possible to combine the velocity vector analyzer with a composition analyzer and determine independently both orbit and composition of any cosmic dust particle.

OPERATION PRINCIPLES OF A VELOCITY VECTOR ANALYZER

The velocity vector $\vec{v}_{vel}$ of a cosmic dust particle, with respect to the instrument's frame of reference, can be completely defined by the coordinates of two points A and B on the particle's trajectory and by the elapsed time for the particle to travel from A to B. Detailed formulae for $\vec{v}_{rel}$ will be given later. $\vec{v}_{rel}$ is transformed into the heliocentric particle velocity $\vec{v}_{hel}$ by taking into consideration the heliocentric spacecraft velocity and the instantaneous orientation of the instrument with respect to the sun. A complete set of orbital parameters for each particle can be obtained from this information. Berg et al. have been utilizing this technique for many years.[1-3]

Uncertainties in the position measurement of the two points introduce the largest errors in the determination of the orbital parameters. Hence, a major effort was devoted to developing a position-sensitive device with a high resolution. A high resolution position-sensitive detector has already been described.[6] While it measures a position only when a dust particle penetrates a thin film,

here we are considering detectors which are based solely on the electrical interaction of a particle's charge with a plane conductor, usually a metallic grid.

Dust particles in interplanetary space carry a positive charge q at an equilibrium surface potential Φ of 5 to 10 volts with respect to the surrounding medium, according to theoretical considerations by Rhee.[7] Even though Jennison and McDonnell did propose an experiment to measure the charge in 1964,[8] it is expected that the solar probe Helios will carry a detector to determine the electrostatic charge of an interplanetary dust particle for the first time.[9]

A particle of radius r carries a charge

$$q = 4\pi \epsilon_0 r \Phi \qquad (1)$$

Table 1 shows typical charges carried by cosmic dust particles. It is clear from Table 1 that one needs not only a most sensitive charge amplifier to detect dust particles with radii as small as 0.01 μm, but also a most effective means of suppressing electromagnetic and acoustic noise. The best amplifiers have presently an electrical noise equivalent to 80 eV (fwhm) in silicon (Kandiah).[10] Radeka and Kraner[11] designed an amplifier for space application with an electrical noise - under optimum conditions - of 125 eV (fwhm) which is equivalent to a charge of 2.2×10^{-18} As (rms). With an amplifier having such a low noise, one can readily detect dust particles carrying charges as small as 1.5×10^{-17} As. Methods of detecting smaller charges, possibly as small as 2.2×10^{-18} As, will be discussed later.

Table 1

Charge q of a particle with radius r and mass m (assuming a density $\rho = 1\,g cm^{-3}$) and equilibrium potential $\Phi = 5$ and 10 volts.

r (μm)		100	10	1	0.1	0.01
m (g)		4×10^{-6}	4×10^{-9}	4×10^{-12}	4×10^{-15}	4×10^{-18}
q (As)	$\Phi = 5$ V	6×10^{-14}	6×10^{-15}	6×10^{-16}	6×10^{-17}	6×10^{-18}
	$\Phi = 10$ V	1.1×10^{-13}	1.1×10^{-14}	1.1×10^{-15}	1.1×10^{-16}	1.1×10^{-17}

EXPERIMENTAL ARRANGEMENT

The experiments were carried out with dust particles from the electrostatic dust accelerator at the Goddard Space Flight Center. A slit at the entrance of the experimental chamber limited the width of the particle beam to approximately 1 mm. The particles carried positive charges q between 10^{-15} and 10^{-13} As and had velocities of several km/s in most cases. The preamplifiers used to perform the experiments were identical to devices flown on Pioneer 10 and 11.[12] The rms noise voltage was 0.23 mV across a feedback capacitor of 1 pF. The power consumption was 10 mW and the weight 9 g excluding shielding material. The amplified signals were displayed on a dual-beam oscilloscope and photographed. The photographs were analyzed by hand, using a millimeter rule. It should be emphasized that either charge or current amplifiers must be used. Voltage amplifiers are not appropriate, since the output of either detector described in this paper must virtually be kept on ac-ground.

POSITION-SENSITIVE DETECTOR USING A CHARGE-DIVIDING TECHNIQUE

The operation of a position-sensitive detector consisting of N sub-detectors and utilizing thin-film penetration[6] can be summarized as follows: A charge q, collected on the k-th sub-detector is divided by a capacitive network into parts q_1 and q_2. In the simplest case, when all capacitors C are equal, the charge coupled to amplifier no. 1 is

$$q_1 = \frac{N + 1 - k}{N + 1} q \tag{2}$$

and the charge coupled to amplifier no. 2 is

$$q_2 = \frac{k}{N + 1} q \tag{3}$$

q_1/q and q_2/q are step functions of the position only, with N possible discrete ratios.

The detector used for this work was made of a plastic frame with a window, 100 mm by 100 mm wide, and 38 parallel tungsten wires with diameters 0.025 mm at equal distances, having an overall transmission coefficient of over 0.99. Any adjacent wires and the two amplifiers were interconnected through a capacitor, C = 560 pF, in parallel with a resistor, R = 10 Megohm, totaling 39 capacitors and 39 resistors which were soldered on terminals located on the frame. While the capacitors made up the actual charge-dividing network, the resistors were used only for the purpose of holding the wires on a defined potential. A schematic diagram is shown in Figure 1.

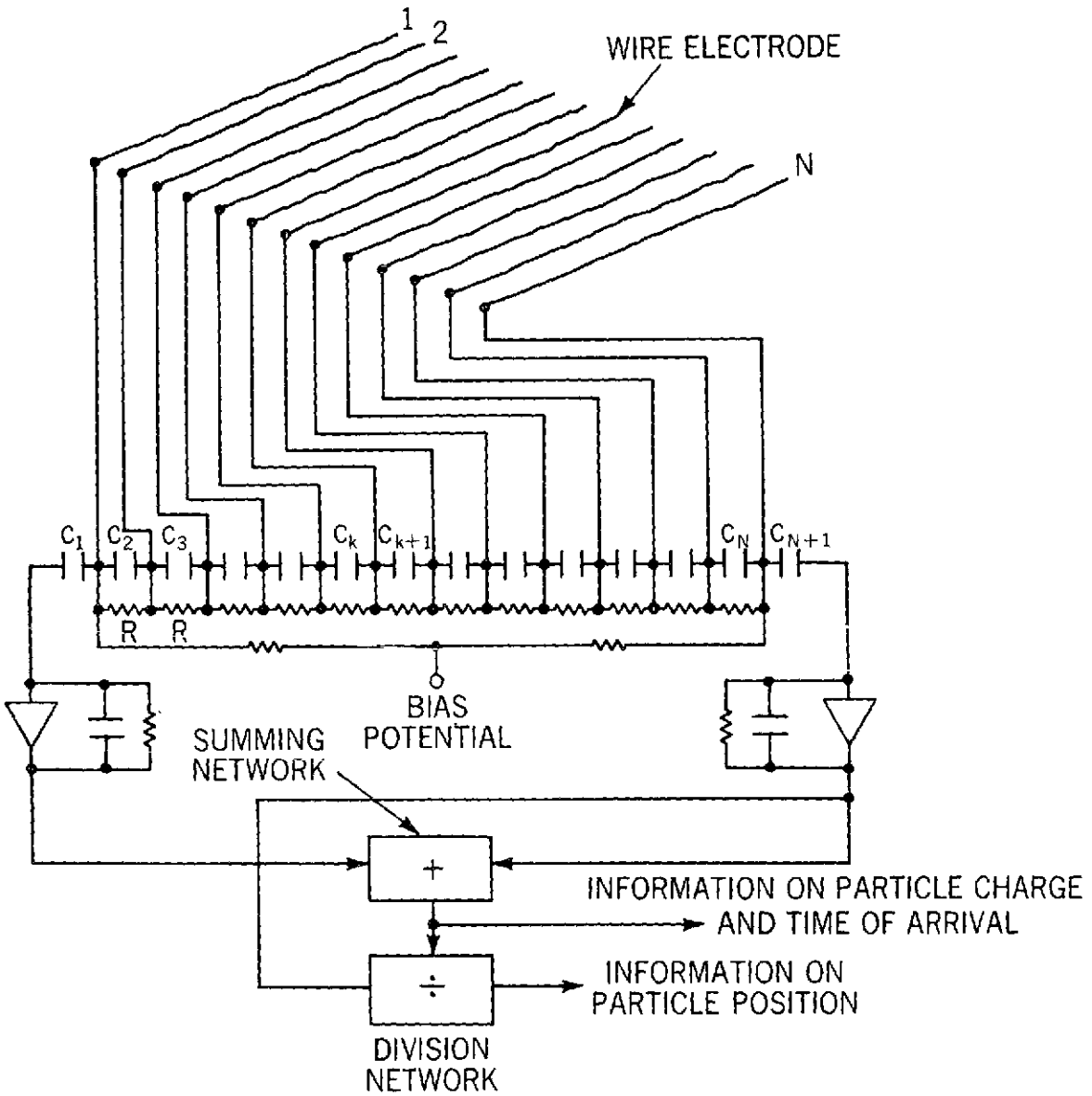

Figure 1. Circuit diagram of a position-sensitive detector with a charge-dividing network

Each end of the charge-dividing network was connected to a charge-sensitive preamplifier. The detector and the two preamplifiers were placed in a grounded metal box having windows covered with knitted tungsten wire mesh for the particles to enter and exit. The outputs of the preamplifiers were fed into laboratory

postamplifiers outside the experimental chamber which performed 7μs RC pulse shaping and final amplification. The noise level after pulse shaping, referred to the preamplifier input, was equivalent to a charge of 3×10^{-17} As.

Each individual pair of wires is a continuous, quasi-linear position-sensitive detector by itself. As a particle passes close to a wire, this wire picks up a strong signal, but the wire next to it picks up a weaker signal. The relative amplitude of a signal is only a function of position. When we assemble many such position-sensitive sub-units through a charge-dividing network, we can combine two principles of position-sensing and obtain a large position-sensitive array which has, at least theoretically, an infinite resolution and an almost linear response.

The results in Figure 2 were obtained by moving the detector in steps of 2 mm through the dust beam in the direction normal to the beam and normal to the wires. Each dot represents a ratio q_1/q, measured from a single particle pass, as a function of the position of the detector. It can be seen that the resolution is 1 - 2 mm or 1 - 2 percent over the entire detector width of 100 mm. The resolution can probably be improved by means of sophisticated electronics like analog-to-digital converters. The curve is linear in the middle region. It is slightly flattened at the two ends. This is due to the fact that the charge of a dust particle is not only sensed at the instant of passage but also before and after that, and the above linear equations, originally derived for a thin-film penetration detector, do not hold exactly.

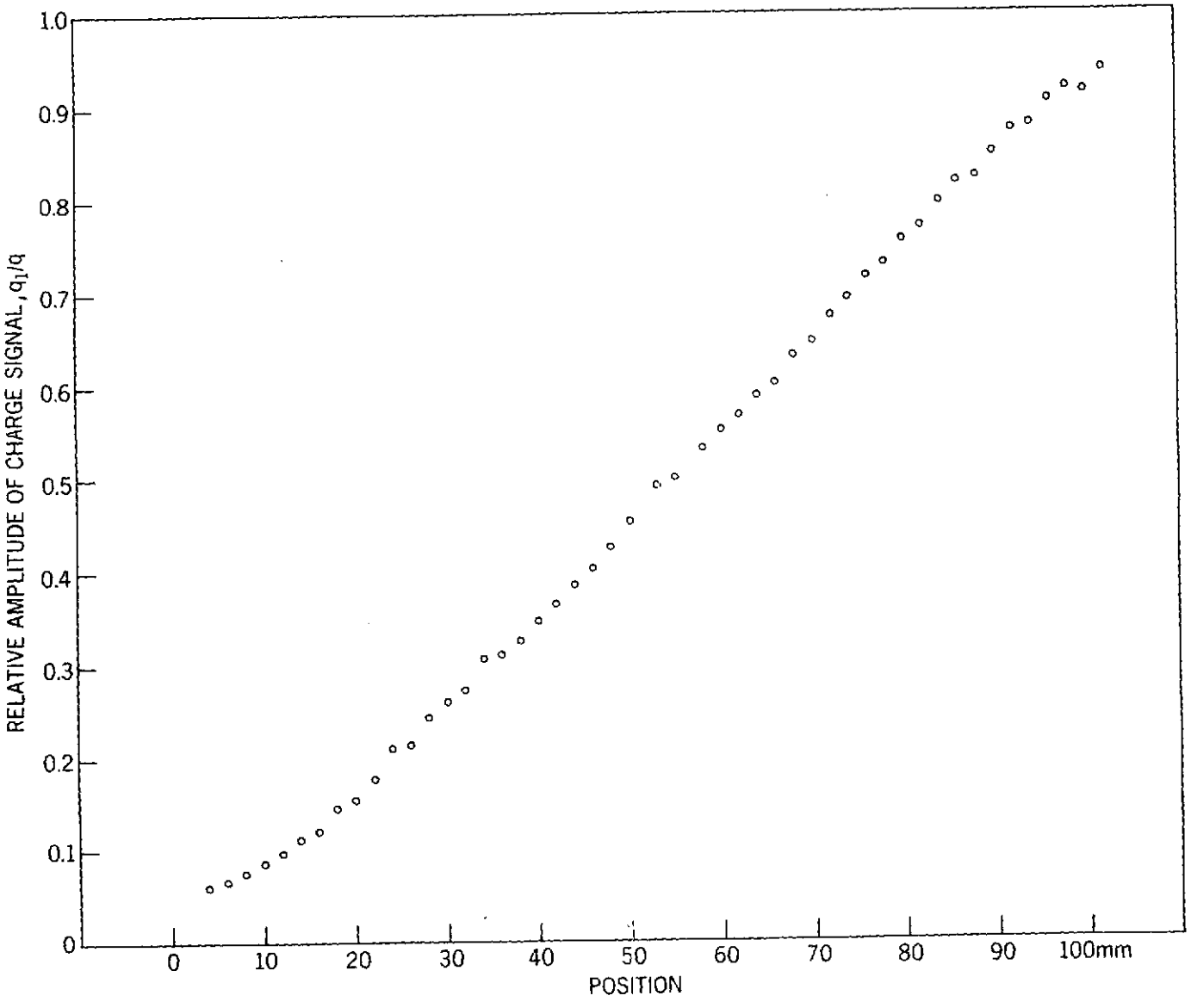

Figure 2. Calibration results of a position-sensitive detector using the charge-dividing technique

MEASUREMENT OF THE VELOCITY VECTOR USING THE CHARGE-DIVIDING TECHNIQUE

A velocity vector analyzer consisting of four position-sensitive detectors in series is shown schematically in Figure 3. Typical overall dimensions are 100 mm by 100 mm by 100 mm, resulting in a viewing angle of approximately 50 degrees. The first and third detectors together measure the angle α between the z-axis and the projection of the trajectory on the x-z-plane,

$$\tan \alpha = \frac{x_2 - x_1}{z_{B1} - z_{A1}} . \tag{4}$$

The second and fourth detectors together measure the angle β between the z-axis and the projection of the trajectory on the y-z-plane,

$$\tan \beta = \frac{y_2 - y_1}{z_{B2} - z_{A2}} . \tag{5}$$

The times when a particle passes through the grids at $z = z_{A1}$, z_{A2}, z_{B1}, and z_{B2} shall be t_{A1}, t_{A2}, t_{B1}, and t_{B2}, respectively. The velocity components are then

$$v_x = \frac{x_2 - x_1}{t_{B1} - t_{A1}} , \tag{6}$$

$$v_y = \frac{y_2 - y_1}{t_{B2} - t_{A2}} , \tag{7}$$

$$v_z = \frac{z_{B1} - z_{A1}}{t_{B1} - t_{A1}} = \frac{z_{B2} - z_{A2}}{t_{B2} - t_{A2}} \tag{8}$$

The velocity vector is

$$\overrightarrow{v_{rel}} = \{v_x, v_y, v_z\} \tag{9}$$

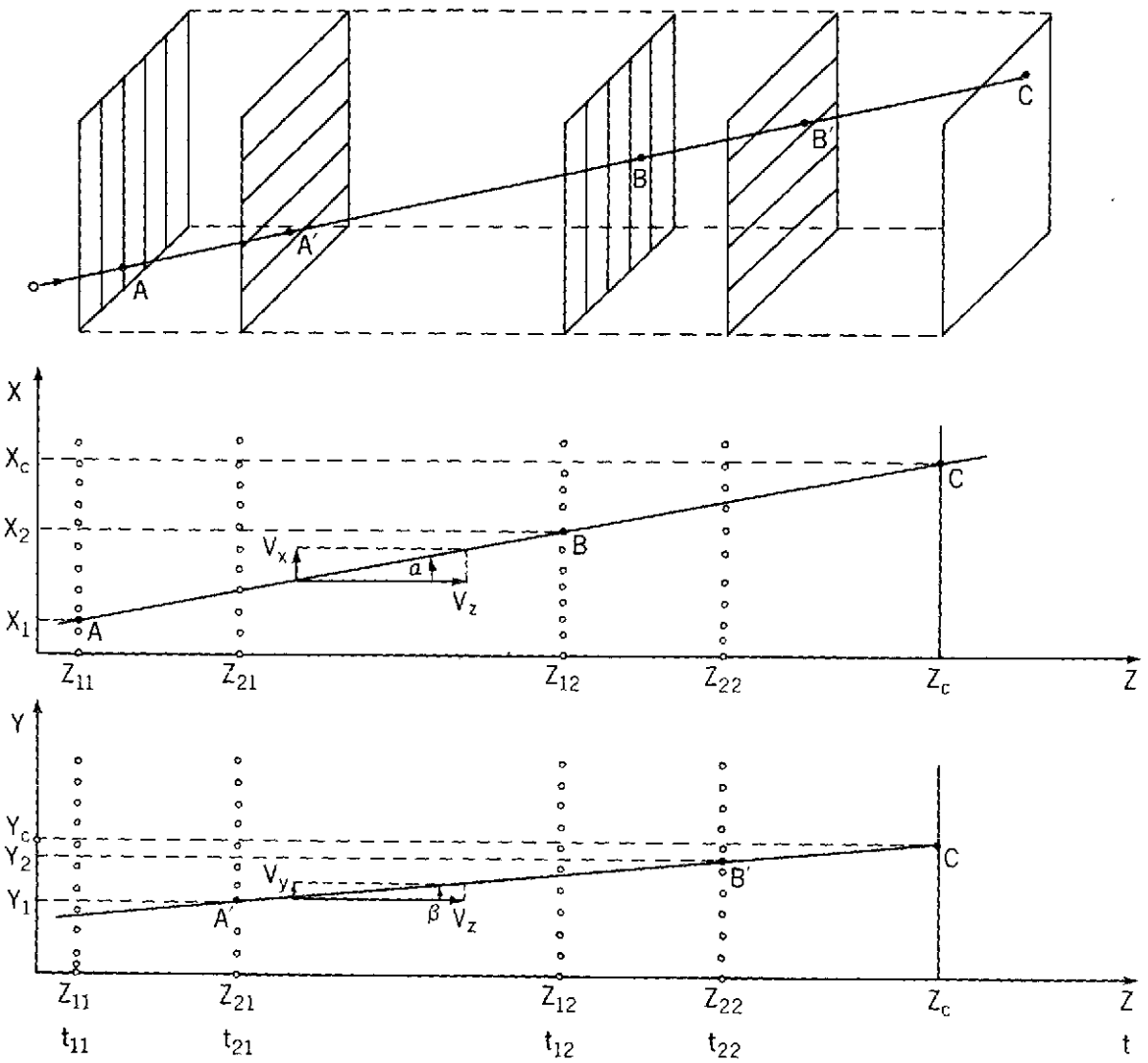

Figure 3. Exploded view of a velocity vector analyzer using the charge-dividing technique. Top: stereographic view. Middle: projection into x-z-plane. Bottom: projection into y-z-plane.

We can also express the coordinates of point C (x_c, y_c, z_c) where the particle trajectory intersects the plane $z = z_c$ which is parallel to the x-y-plane at an arbitrary distance z_c,

$$x_c = x_1 + (z_c - z_{A1}) \tan \alpha \tag{10}$$

$$y_c = y_1 + (z_c - z_{A2}) \tan \beta \tag{11}$$

The overall transmission coefficient of the four grids is over 0.96. For use in a space experiment, however, the parallel metallic wires would have to be interwoven perpendicularly with non-metallic thread, such as nylon, in order to strengthen the grid mechanically without shortening the wires electrically. The transmission coefficient would therefore be about 0.92.

It is clear that any noise superimposed on the signal will affect the accuracy with which the relative amplitudes q_1/q and q_2/q are measured. In order to achieve a resolution of 1 percent in position, the signal-to-noise ratio must be considerably better than 100. This condition may not be met for the charge signals from submicron size particles and, therefore, their orbits can probably not be measured with the full precision. The detector described next will be much more adequate to measure orbits of submicron size particles.

POSITION-SENSITIVE DETECTOR USING A TIME-OF-FLIGHT TECHNIQUE

A second detector has been constructed with three grids placed in a shielded box as shown in Figure 4. Each grid was made of a metal frame with a window, 100 mm by 100 mm wide. Knitted wire mesh was stretched over the frame and glued in place with conductive epoxy. The mesh had been knitted from 0.012 mm thick tungsten wire. It is a strong and almost indestructible material despite its cobweblike thinness. The hole size was between 1 and 2 mm, giving a transmission coefficient of 0.98 to 0.99. Due to stretching, the mesh was held under a permanent tension such that it made a well-defined plane with the frame. The

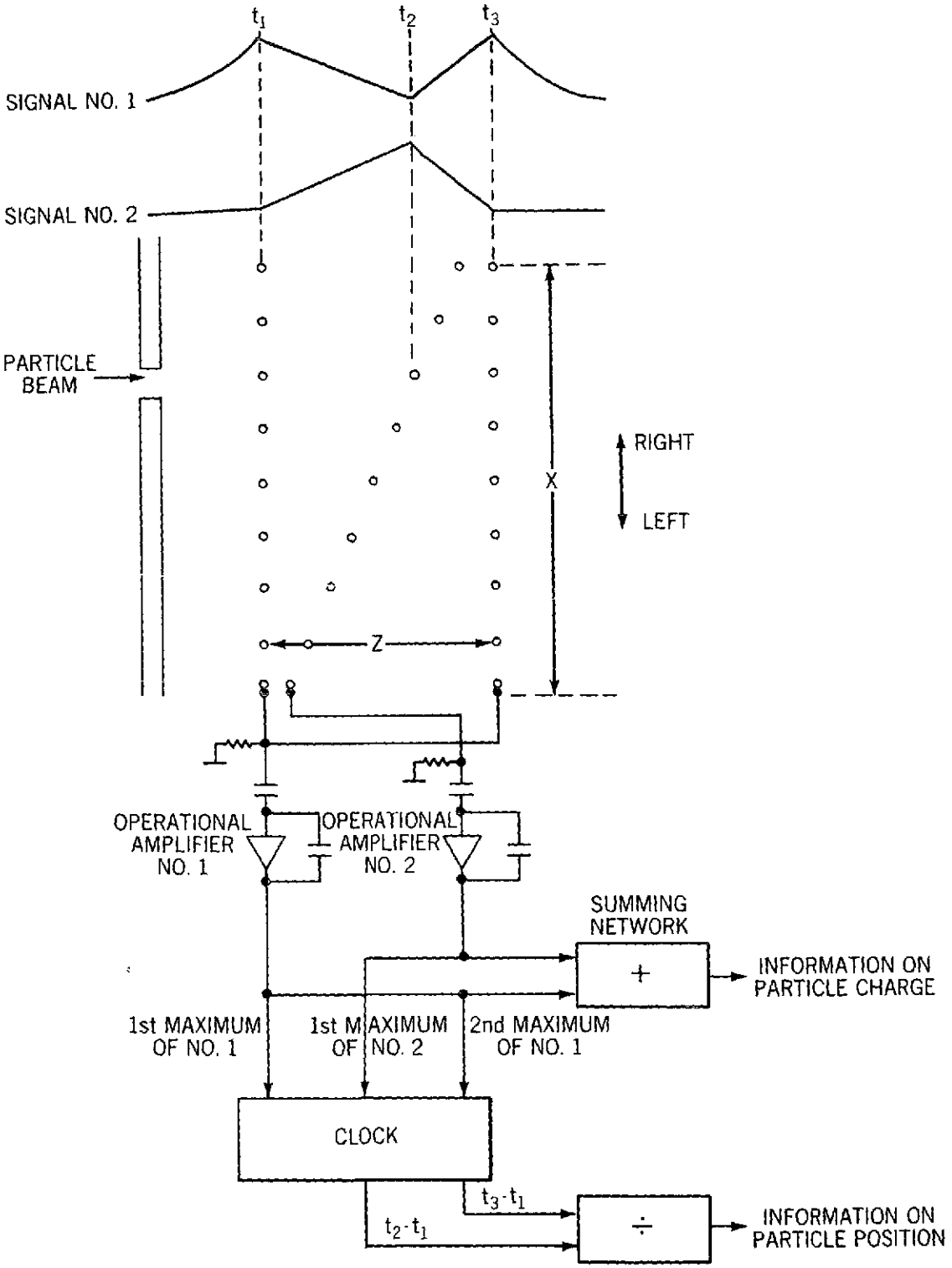

Figure 4. Circuit diagram of a position-sensitive detector using the time-of-flight technique

first and third grids were parallel to each other and perpendicular to the beam, both being connected to amplifier no. 1. The second grid was inclined by about 19 degrees relative to the first grid and connected to amplifier no. 2. No pulse shaping was made in order to preserve the shapes of the signals. The grids have been placed together as close as possible, so that the angle γ between the first and second grids was virtually given by $\tan \gamma = Z/X$.

When a particle passes through the detector, its charge q is first sensed by amplifier no. 1. The first maximum of this signal is reached at time t_1 when the particle penetrates the first grid. As it leaves the first and approaches the second grid, this signal drops and the signal from amplifier no. 2 rises. When the particle penetrates the second grid, at time t_2, the signal from no. 2 is at its maximum; but the particle charge is shielded from the first and third grid, so the signal from no. 1 is zero. As the particle approaches the third grid, the signal from no. 2 drops and the signal from no. 1 rises. The second maximum of the signal from no. 1 is reached at time t_3 when the particle penetrates the third grid. An example of a pair of signals is shown in Figure 5. We realize: the more left the particle passes the shorter is the time $t_2 - t_1$; the more right it passes the longer is $t_2 - t_1$. Hence, while the time $t_3 - t_1$ tells us the velocity of a particle, the time $t_2 - t_1$, divided by $t_3 - t_1$, tells us the position of passage. Figure 6 shows the ratio $(t_2 - t_1)/(t_3 - t_1)$ measured as a function of position. The results form a straight line within the experimental uncertainties. It can be seen that the resolution of this detector is approximately 1 mm over the entire detector width of 100 mm.

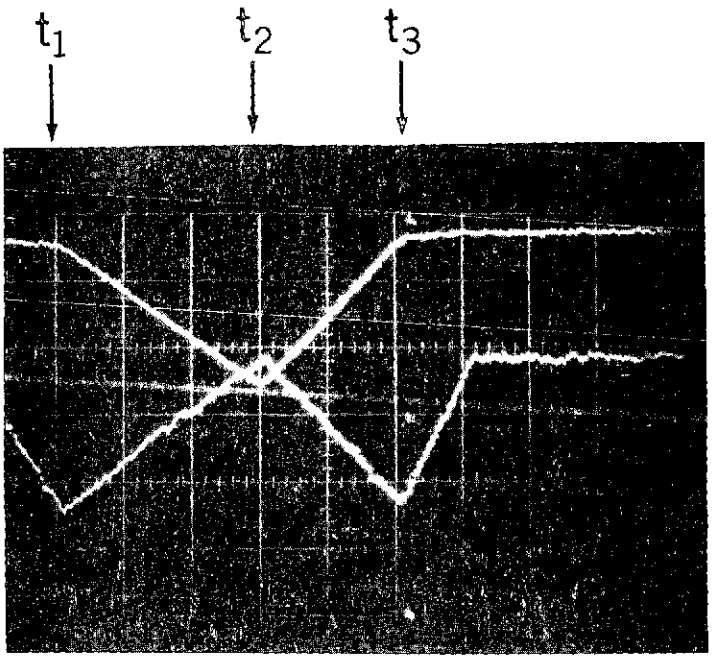

Figure 5. Oscilloscope trace of the signals from a position-sensitive detector using the time-of-flight technique (5μs/div., 10 mV/div.). Note that the lower signal is noisier than the upper signal by a factor of 3, due to different noise figures of the two preamplifiers. The polarity has been reversed by the amplifiers.

MEASUREMENT OF THE VELOCITY VECTOR USING THE TIME-OF-FLIGHT TECHNIQUE

A velocity vector analyzer again consists of four position-sensitive detectors in series. As shown in Figure 7, we may use five parallel grids, at distances Z from each other, and connect them to amplifier no. 1. We put four inclined grids between the parallel grids, such that they almost touch them, and connect them to amplifier no. 2. We measure electronically the time intervals t_1, t_X, and t_Z, for reference see Figure 7. The detector height X is known. The

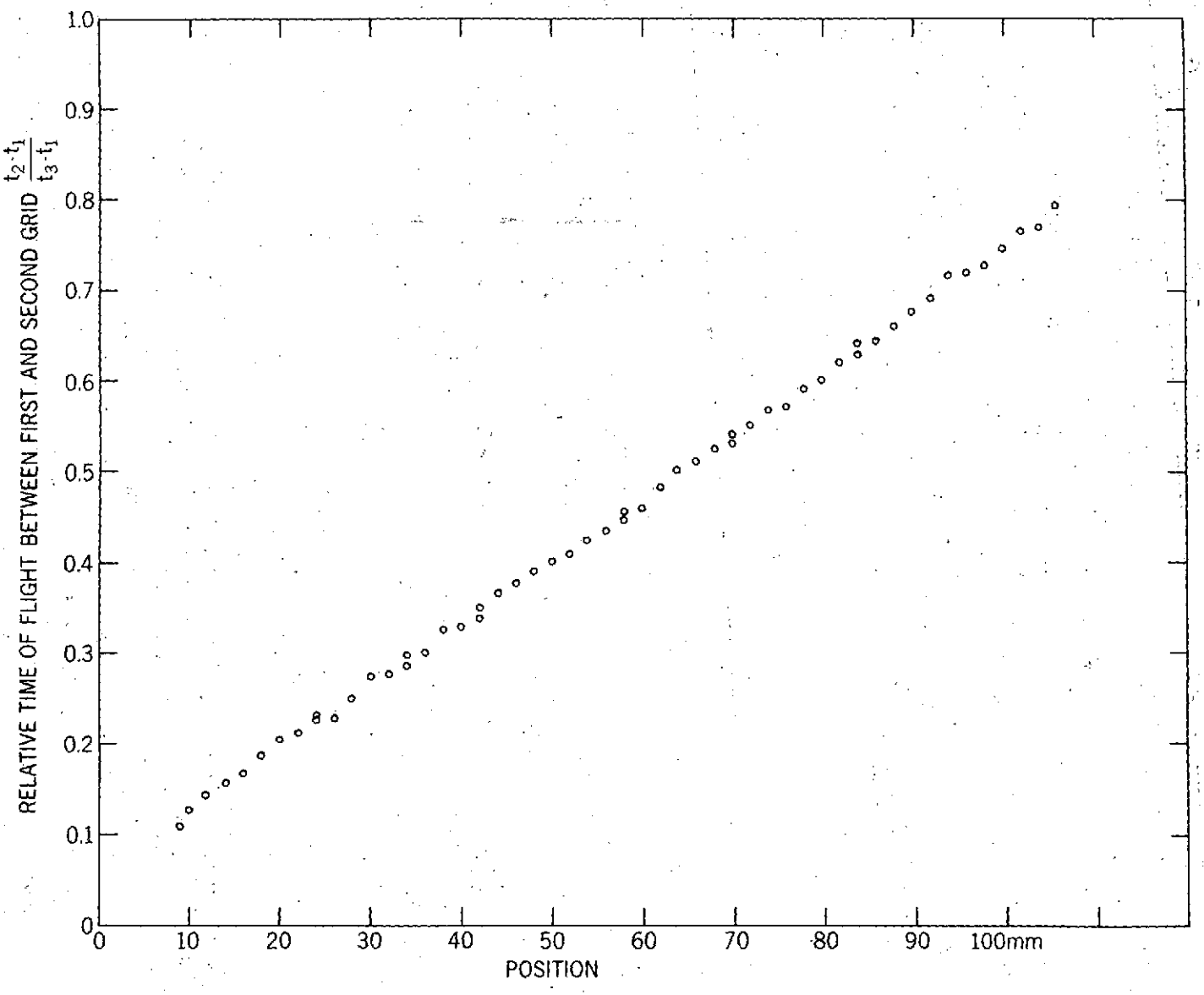

Figure 6. Calibration results of a position-sensitive detector using the time-of-flight technique

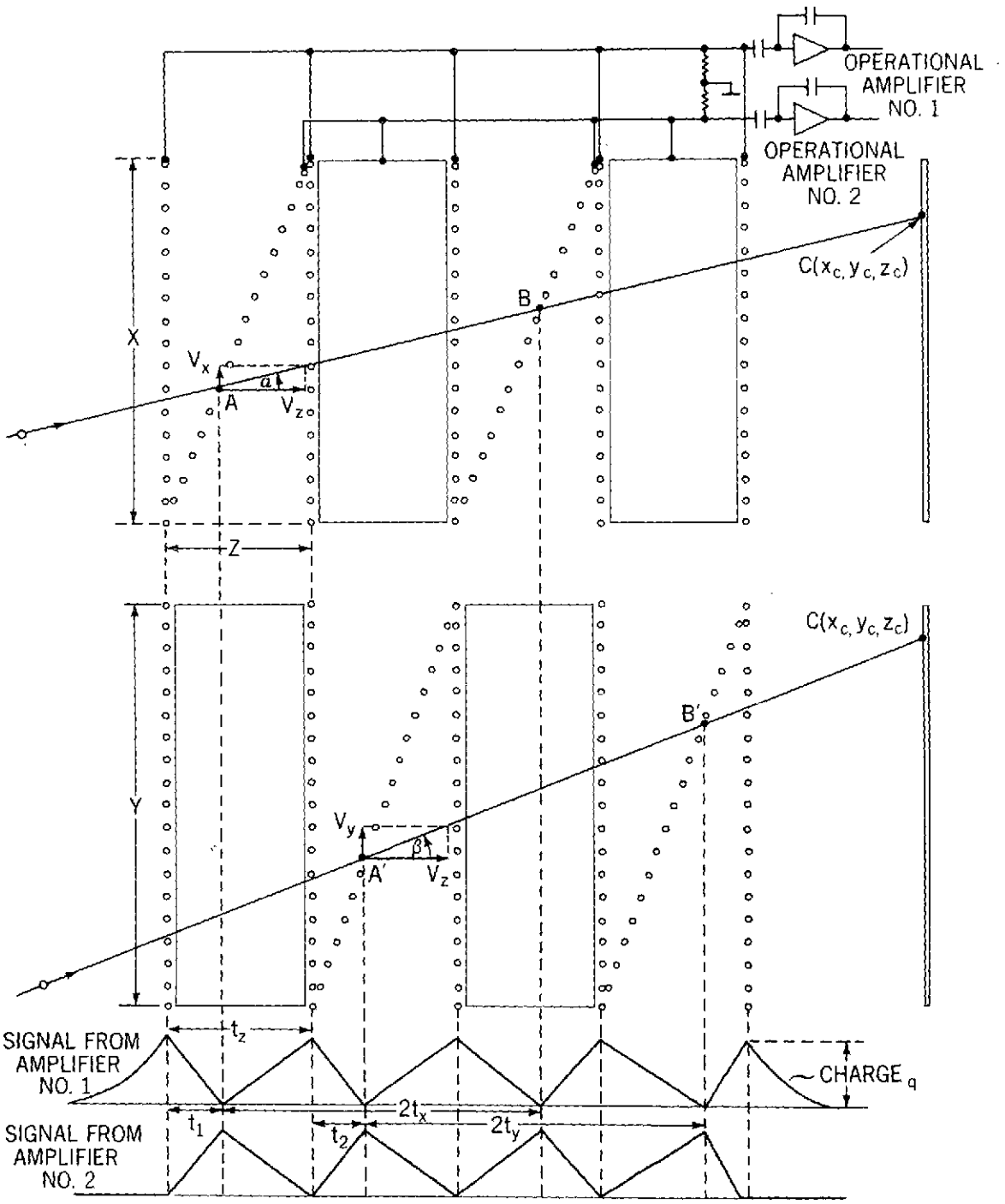

Figure 7. Schematic diagram of a velocity vector analyzer using the time-of-flight technique. Top: projection into x-z-plane. Bottom: projection into y-z-plane

velocity components parallel to the x- and z-axes are, respectively,

$$v_z = \frac{1}{t_z} Z \tag{12}$$

$$v_x = \left(\frac{1}{t_z} - \frac{1}{t_x}\right) X \tag{13}$$

For the angle α between the z-axis and the projection of the trajectory on the x-z-plane we obtain

$$\tan \alpha = \left(1 - \frac{t_z}{t_x}\right) \frac{X}{Z} \tag{14}$$

Considering the y-z-plane, we get similar relations when t_2 and t_y are measured and the detector width Y is known. The velocity component parallel to the y-axis is

$$v_y = \left(\frac{1}{t_z} - \frac{1}{t_y}\right) Y \tag{15}$$

For the angle β between the z-axis and the projection of the trajectory on the y-z-plane we obtain

$$\tan \beta = \left(1 - \frac{t_z}{t_y}\right) \frac{Y}{Z} \tag{16}$$

We can also express the coordinates of point C (x_c, y_c, z_c), where the particle trajectory intersects the plane $z = z_c$, which is parallel to the x-y-plane at an arbitrary distance z_c from the first grid,

$$x_c = \frac{X\, t_1}{Z\, t_x} + \frac{X}{Z} \left(1 - \frac{t_z}{t_x}\right) z_c \tag{17}$$

$$y_c = \frac{Y\,(t_2 + t_z)}{Z\,t_y} + \frac{Y}{Z}\left(1 - \frac{t_z}{t_y}\right) z_c \qquad (18)$$

The overall transmission coefficient of the nine grids is between $0.98^9 = 0.83$ and $0.99^9 = 0.91$. Typical dimensions of the instrument are: width = 100 mm, height = 100 mm, length = 160 mm. The resulting viewing angle is approximately 32 degrees.

An experiment designed to verify the angular measurement has been performed with an arrangement of five grids as sketched in Figure 8. The dimensions

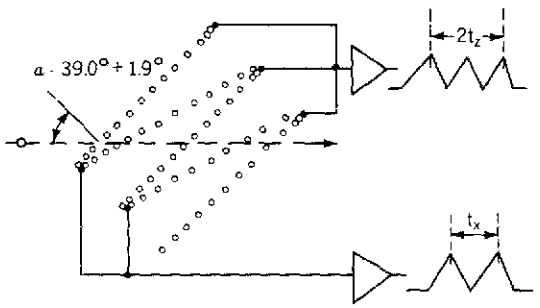

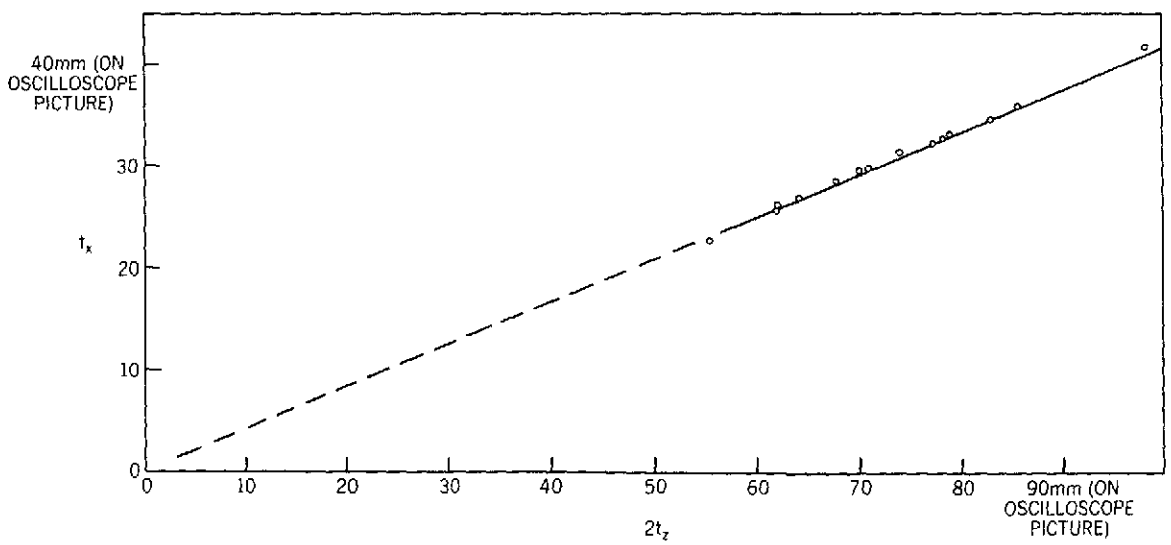

Figure 8. Experimental arrangement and measured results of an angular detector using the time-of-flight technique

were approximately X = Y = 100 mm, Z = 25 mm, and an angle of about 40 degrees was chosen between the sensor axis and the beam. Time intervals t_x and $2t_z$ were taken from photographs of 18 oscilloscope recordings and plotted in the diagram of Figure 8. Equation 14 gives $\alpha = 39.0 \pm 1.9$ degrees. The uncertainty can be explained solely by the error which is introduced when measuring t_x and $2t_z$ with a millimeter rule on a photograph.

A redundant measurement of the velocity vector can be made by using 13 grids, the arrangement being sketched in Figure 9. The transmission coefficient of all

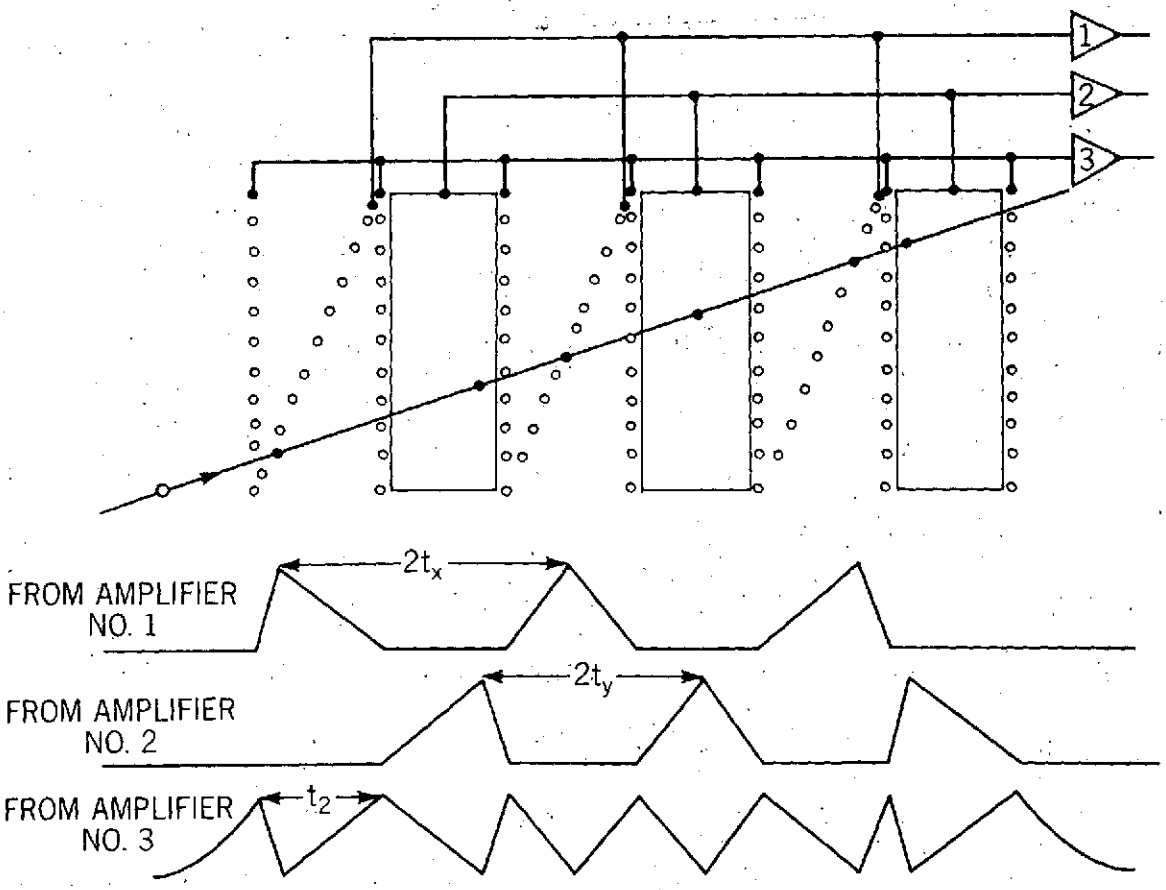

Figure 9. Schematic diagram of a velocity vector analyzer modified for the detection of dust particles with extremely small charges

grids together would be between 0.77 and 0.88. The viewing angle is about 22 degrees. The employment of three amplifiers appears to be advantageous. The time intervals t_x, t_y, and t_z between the maxima of any of the three signals are constant. According to equations 12, 13, and 15, those time intervals give directly the three velocity components v_x, v_y, v_z.

This fact will help us in measuring the velocity vectors of particles carrying charges as small as 2.2×10^{-18} As, as will be discussed later. The presumedly high flux of very small cosmic dust particles entirely compensates for the reduced viewing angle to give a high rate of particle detection.

RELATIVE ADVANTAGES AND DISADVANTAGES OF THE TWO TECHNIQUES

Charge-Dividing Technique

The major advantage is the large field of view that the velocity vector analyzer has. The major disadvantage is the reduced resolution for submicron size particles.

Time-of-Flight Technique

The only disadvantage is the smaller viewing angle. There are several advantages. Mechanically, all grids are easy to manufacture and to align and are almost indestructible. There are no electronic components to be mounted on any frame. A high reliability is, therefore, inherent. The pulses obtained have equal amplitudes, and certain maxima and minima have equal distances t_z. The slopes of the pulses are nearly linear. The calibration curve is linear. All

these facts help to distinguish small signals from noise pulses. Furthermore, it is easier, electronically, to measure time intervals than pulse heights. Some of these relative features are listed in Table 2.

Table 2

Comparison of the Two Techniques

Technique	Charge-Division	Time-of-Flight
Mechanical Construction	more difficult and vulnerable	simpler, rugged
Electronic Design	more difficult	simpler
Number of Preamplifiers	8	2
Reliability	medium	high
Sensitivity for Small Charges	medium	high
Field of View	larger	smaller

An advantage of both techniques is the freedom in choosing the bias potential of the grids. The optimum choice is normally to have all potentials on spacecraft ground. Then the spaces between grids are entirely field-free and no acoustic noise can be generated by vibrating grids, an effect frequently observed with impact plasma detectors.

ACCURACY OF MEASUREMENT OF ANGLES OF INCIDENCE

The calibration experiments described above show that the detectors have a resolution with respect to position of $\Delta x = 1 - 2$ mm over a width of 100 mm.

If we measure the coordinates of two points on a particle trajectory which are separated by a distance Z, we obtain an angular resolution

$$\Delta\alpha \leq \arctan \frac{\Delta x}{Z} \tag{19}$$

If $Z = 100\,\text{mm}$, we obtain $\Delta\alpha \leq 0.57 - 1.14$ degree, where the = sign is for normal incidence and the $<$ sign is for oblique incidence. A higher resolution can be achieved by increasing Z and/or decreasing Δx. Similar relations hold for the angular resolution $\Delta\beta$.

ACCURACY OF THE MEASUREMENT OF THE VELOCITY COMPONENTS

Charge-Dividing Technique

If we add errors quadratically, we get the errors of the velocity components,

$$\frac{\Delta v_x}{v_x} = \left\{ \left(\frac{\Delta x_1}{x_1}\right)^2 + \left(\frac{\Delta x_2}{x_2}\right)^2 + \left(\frac{\Delta t_{A1}}{t_{A1}}\right)^2 + \left(\frac{\Delta t_{B1}}{t_{B1}}\right)^2 \right\}^{1/2} \tag{20}$$

$$\frac{\Delta v_y}{v_y} = \left\{ \left(\frac{\Delta y_1}{y_1}\right)^2 + \left(\frac{\Delta y_2}{y_2}\right)^2 + \left(\frac{\Delta t_{A2}}{t_{A2}}\right)^2 + \left(\frac{\Delta t_{B2}}{t_{B2}}\right)^2 \right\}^{1/2} \tag{21}$$

$$\frac{\Delta v_z}{v_z} = \left\{ \left(\frac{\Delta z_{A1}}{z_{A1}}\right)^2 + \left(\frac{\Delta z_{B1}}{z_{B1}}\right)^2 + \left(\frac{\Delta t_{A1}}{t_{A1}}\right)^2 + \left(\frac{\Delta t_{B1}}{t_{B1}}\right)^2 \right\}^{1/2} \tag{22}$$

Having $$\frac{\Delta x_1}{x_1} = \frac{\Delta x_2}{x_2} = \frac{\Delta y_1}{y_1} = \frac{\Delta y_2}{y_2} = (1 - 2) \times 10^{-2},$$

$$\frac{\Delta z_{A1}}{z_{A1}} = \frac{\Delta z_{A2}}{z_{A2}} = \frac{\Delta z_{B1}}{z_{B1}} = \frac{\Delta z_{B2}}{z_{B2}} = 5 \times 10^{-3}, \text{ and}$$

$$\frac{\Delta t_{A1}}{t_{A1}} = \frac{\Delta t_{A2}}{t_{A2}} = \frac{\Delta t_{B1}}{t_{B1}} = \frac{\Delta t_{B2}}{t_{B2}} = 5 \times 10^{-3}$$

$$(\text{for } t_{B1} - t_{A1} \geq 2\,\mu s \text{ and } \Delta t = 10\,ns),$$

we obtain

$$\frac{\Delta v_x}{v_x} = \frac{\Delta v_y}{v_y} = (1.6 - 2.9) \times 10^{-2} \text{ and}$$

$$\frac{\Delta v_z}{v_z} = 10^{-2}$$

Time-of-Flight Technique

In a similar approach we obtain

$$\frac{\Delta v_x}{v_x} = \left\{ \left(\frac{\Delta t_x}{t_x}\right)^2 + \left(\frac{\Delta t_z}{t_z}\right)^2 + \left(\frac{\Delta X}{X}\right)^2 \right\}^{1/2} \tag{23}$$

$$\frac{\Delta v_y}{v_y} = \left\{ \left(\frac{\Delta t_y}{t_y}\right)^2 + \left(\frac{\Delta t_z}{t_z}\right)^2 + \left(\frac{\Delta Y}{Y}\right)^2 \right\}^{1/2} \tag{24}$$

$$\frac{\Delta v_z}{v_z} = \left\{ \left(\frac{\Delta t_z}{t_z}\right)^2 + \left(\frac{\Delta Z}{Z}\right)^2 \right\}^{1/2} \tag{25}$$

If we have an accuracy of timing ($\Delta t_x = 10\,ns$, $t_x \geq 2\,\mu s$) of

$$\frac{\Delta t_x}{t_x} = \frac{\Delta t_y}{t_y} = \frac{\Delta t_z}{t_z} \leq 5 \times 10^{-3}$$

and a stability of instrumental dimensions ($\Delta X = 0.5\,mm$, $X = 100\,mm$)

$$\frac{\Delta X}{X} = \frac{\Delta Y}{Y} = \frac{\Delta Z}{Z} = 5 \times 10^{-3},$$

then the errors of the velocity components are

$$\frac{\Delta v_x}{v_x} = \frac{\Delta v_y}{v_y} \leq 8.7 \times 10^{-3} \quad \text{and} \quad \frac{\Delta v_z}{v_z} \leq 7.1 \times 10^{-3}.$$

ON THE ACCURACY OF DETERMINATION OF ORBITAL ELEMENTS OF COSMIC DUST PARTICLES

For the purpose of demonstrating the potential of a high resolution velocity vector analyzer, let us consider the cosmic dust particle that has been recorded with Pioneer 9 on October 11, 1969. Due to the combined uncertainty of velocity (±18 percent) and angle of incidence (±25 degrees), the perihelion distance of its orbit can have been anything between 4.2×10^{-4} and 9.2×10^{-1} a.u.[13] or 0.09 and 196 solar radii, as shown in Figure 10. The question remains unanswered whether the particle has been ejected from the solar atmosphere (perihelion distance equal or less than 1 solar radius) or whether it is a fragment from a collision process that happened in the vicinity of the sun (perihelion distance larger than 1 solar radius).

Two calculations can be made to show the improvement possible. In the first calculation it is assumed that the particle had the nominal velocity, mass, and angles of incidence as recorded with Pioneer, but the uncertainties were only as small as those claimed in this paper, ±1 percent in velocity and ±1 degree in angle. The range of resulting orbits is shown in Figure 10, too. Possible perihelion distances are only from 2.4 to 4.0 solar radii. In the second calculation, we assume a nominal velocity and a velocity resolution as before and ask for the angle that would be observed at 1 a.u. between the orbits of particles with perihelion distances of zero (assuming the solar mass to be concentrated in a point)

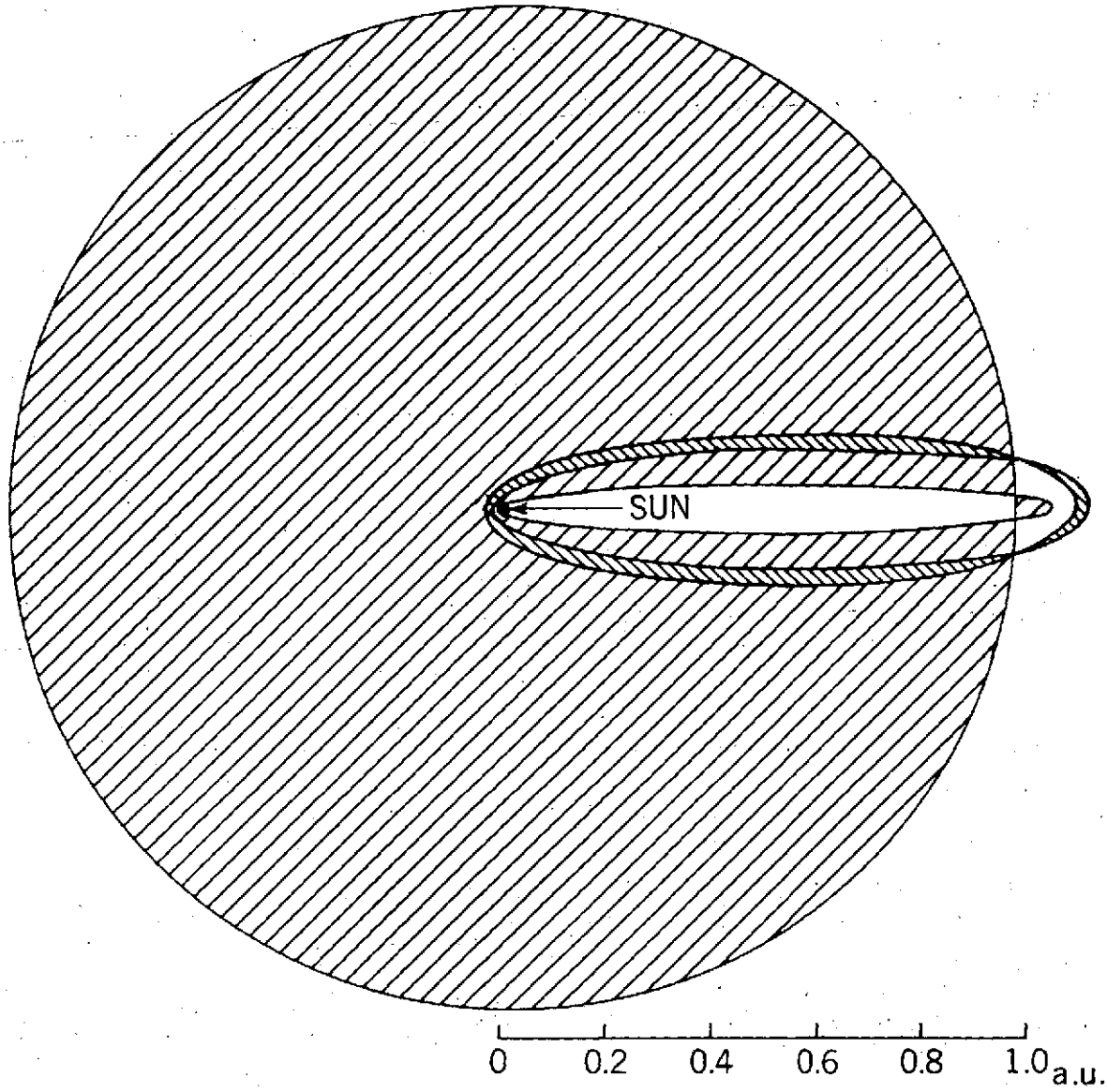

Figure 10. Possible orbits of a cosmic dust particle recorded with Pioneer 9 (light shaded region) as compared with orbits that could have been recorded if the new methods would have been available for the Pioneer 9 measurement (dark shaded region)

and 1 solar radius. If we take into account only gravitational forces, we find an angle of about 10 degrees between the two orbits, which can readily be resolved with the new methods.

We conclude that with a velocity vector analyzer one would indeed be able to answer the question on the origin of dust particles coming from the direction of the sun.

APPLICATION OF THE NEW TECHNIQUES TO SUPPORT COSMIC DUST COLLECTION EXPERIMENTS

Numerous experiments have been made in the past and are planned in the future in order to collect cosmic dust particles from space and to bring them into the laboratory for investigation. Once a collector surface is in the laboratory, a most time-consuming task is locating particles by means of an optical or electron microscope. This task would be greatly facilitated if the impact positions of the particles can be recorded electronically while the collector is being exposed to space. Knowing not only the location but also the velocity, obliquity, and time of impact of each particle would be very helpful for the interpretation of the laboratory measurements. This can be achieved by placing a velocity vector analyzer in front of the collector surface.

COMBINATION OF A VELOCITY VECTOR ANALYZER WITH A COMPOSITION ANALYZER

Composition analyzers for cosmic dust particles have been described elsewhere.[9, 14, 15, 16, 17] A composition analyzer is to fly in space for the first time on the solar probe Helios.[9] Such an analyzer can readily be placed behind a velocity vector analyzer. A cosmic dust particle would first pass through the velocity

vector analyzer. One would be able to calculate the orbit from the velocity vector and could, at least in many cases, identify the dust source (comet, asteroid, the moon, the sun, interstellar dust cloud, etc.). Then the particle would enter the composition analyzer, being partly vaporized and ionized and a mass spectrum of the ions would be taken, indicating the particle's composition. Evaluating the composition would result in conclusions on the particle's history and the abundance of elements in the source. Such a universal set of parameters of a cosmic dust particle could never before be measured simultaneously.

Combining composition (such as on Helios) and velocity vector analyzers (such as on Pioneer 8 and 9 and Apollo 17) has not been advisable in the past because every dust particle had to penetrate a thin film in order that its velocity vector could be measured. The penetration has the following adverse effects on a dust particle:

- Its velocity tends to be diminished
- Its angles of incidence tend to be altered
- Its mass tends to be reduced
- It may break up into several fragments which would arrive in the composition analyzer at different times, producing overlapping mass spectra
- Some mass from the film tends to be ejected and to hit other parts of the detector
- Its mineralogical structure tends to be altered
- Its chemical composition is falsified if the particle picks up material from the film

All of these effects can be avoided in future experiments because of the high transmission coefficient of the velocity vector analyzer.

The front plate of the composition analyzer can be made a two-dimensional position-sensitive detector with a high resolution as described in reference 16. Then the second half of the velocity vector analyzer can be omitted resulting in a large viewing angle and a high transmission.

ON THE SCIENTIFIC IMPORTANCE OF MEASURING CHARGES OF COSMIC DUST PARTICLES

So far we have considered the fact that cosmic dust particles usually carry an electric charge only as means to measure the velocity vector. An important by-product is the measurement of the charge itself. Due to the charge carried by a very small ($\leq 0.1 \mu m$) cosmic dust particle, its orbit can be disturbed by the presence of electric or magnetic fields in space.[18, 19, 20, 21, 22] Because charged dust particles have a large cross section for electrons and protons, they can be coupled to the solar wind.[21, 23, 24] Those and other effects could be studied in situ.

A reason why such studies have only recently become possible is because considerable progress has been made in improving the noise performance of charge amplifiers. At the same time, the ability to suppress electromagnetic interferences on a spacecraft has been perfected, which has been a problem in the past.

DETECTION OF CHARGE SIGNALS IN NOISE

When looking for small signals, one normally sets the lowest threshold so high above the noise level that false alarms due to large noise spikes are extremely seldom (e.g., less than 1 per year). If certain features of a signal are known, however, as in the case of the velocity vector analyzer using the time-of-flight technique, the threshold can be lowered, see e.g., reference 25. We can design a velocity vector analyzer based on the time-of-flight technique, as shown in Figure 7, followed at distance z_c by a very sensitive impact detector, such as a plasma detector with an electron multiplier for ion or electron detection, so that virtually all particles of interest are detected with a high level of confidence. Then we know the following about the signals from the velocity vector analyzer:

1. The charge signals occurred shortly before the impact, the time lapse being $\Delta t_c = z_c/v_z$.
2. The time intervals between consecutive maxima of the signal from amplifier no. 1 are equal, namely Z/v_z.
3. All maxima have equal heights.
4. Between the maxima, the voltage always drops to zero.
5. The slopes of the signals, both rising and falling are nearly linear.
6. The signals from the two amplifiers are complementary; i.e., when one is falling, the other is rising, and vice versa, such that the sum is constant at any instant, as long as the dust particle is inside the velocity

vector analyzer; in particular, the maxima of one signal coincide with the minima of the other.

In order to preserve the information that is contained in the signals, they must be stored continuously, by means of either a delay line or an analog shift register, until the impact detector has confirmed the arrival of a dust particle. After the particle impact has been detected, the stored analog information must be digitized and either processed by an on-board computer or transmitted to ground for later processing.

A simple mathematical simulation experiment has been made with a desk calculator, based only on items 1 and 2 above. A noisy signal has been constructed by adding white noise from tabulated random normal numbers[26] to an idealized signal similar to one from a velocity vector analyzer; see Figure 11 (top). The ratio between signal amplitude and noise voltage (rms) was chosen to be unity. Figure 11 (bottom) shows the autocorrelation function of the noisy signal. The periodicity of the underlying signal becomes apparent. The velocity component v_z can directly be calculated from the period of the autocorrelation function. A similar calculation performed with the signal from amplifier no. 2 can be used to confirm and to improve the results derived from the first signal. By adding a third amplifier and four more grids for a redundant measurement, as in the arrangement of Figure 9, the detection of signals in noise becomes still more effective. This simulation experiment, although far from being perfect, shows

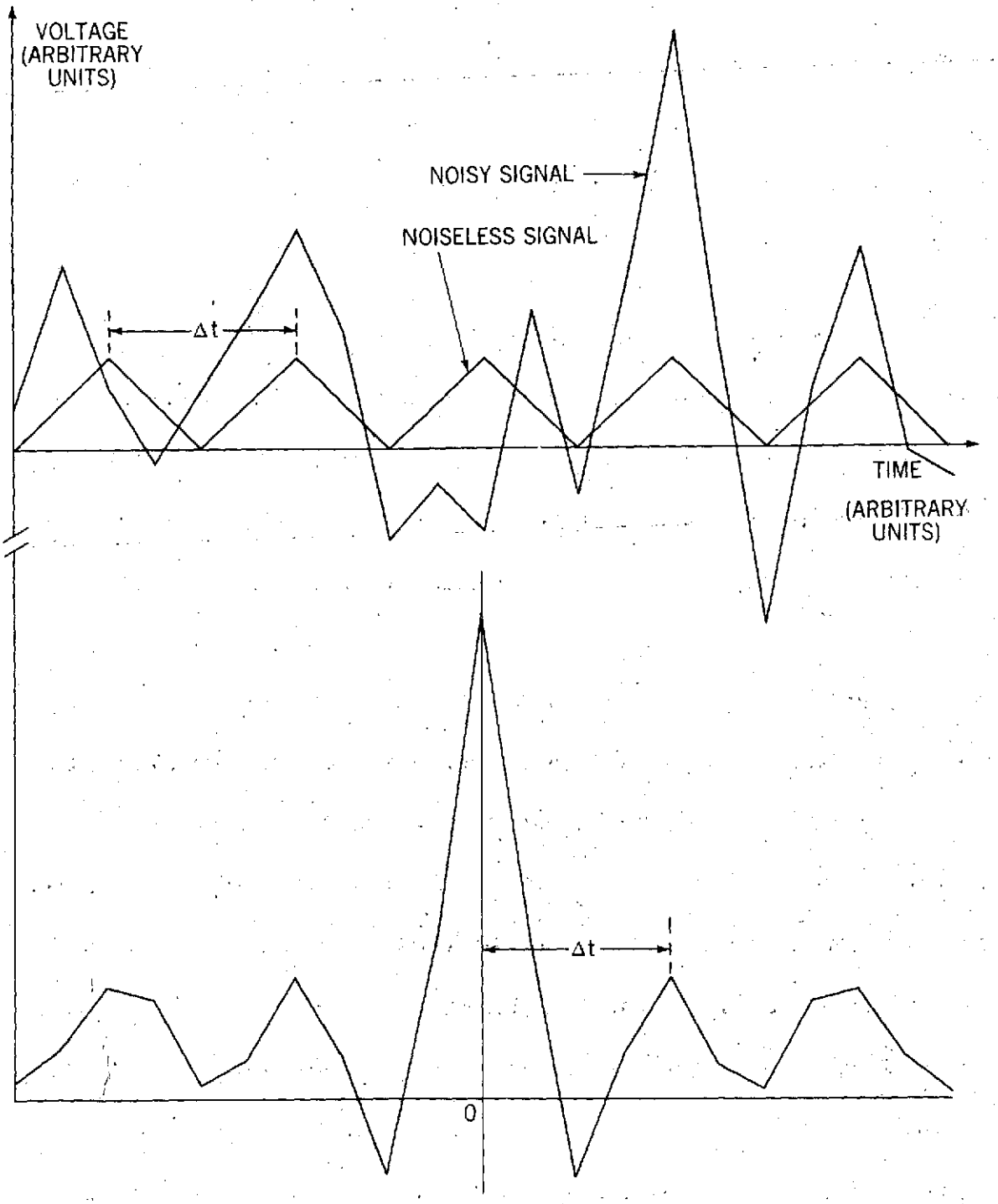

Figure 11. A noisy signal constructed by adding an idealized noiseless signal to white noise (top). The autocorrelation function of the noisy signal reveals the underlying periodicity of the original signal (bottom).

that much information can be extracted from the signals of the velocity vector analyzer, even if the signal-to-noise ratio is of the order of unity. We apply this result to a state-of-the-art charge amplifier[11] with an equivalent noise charge of 2.2×10^{-18} As and conclude that one could analyze trajectories of particles with charges of the order of 2.2×10^{-18} As.

RANGE OF MEASURABLE PARTICLE SIZES AND VELOCITIES

Figure 12 shows the range of particle masses m and velocities v measurable with the HEOS 2 micrometeoroid experiment[9] and that of a time-of-flight velocity vector analyzer. Since the HEOS detector measures the quantity $mv^{3.5}$, the mass range varies strongly with velocity. As a result, particles having either small masses and low velocities (e.g., $m = 10^{-12}$ g, v = 2 km/s) or large masses and high velocities (e.g., $m = 10^{-12}$ g, v = 50 km/s) fall outside the measurement range. The velocity vector analyzer provides a signal amplitude that is independent of the particle velocity. We choose a range of velocities from 1 to 80 km/s, although the tests have only been performed at a few km/s. Neither lower nor upper limit is a firm limit but can be extended by adapting the electronics, the dimensions of the instrument, and/or by relaxing the requirement of a precision of 1 percent in velocity measurement. If our amplifier has the same dynamic range as that in the HEOS experiment, 1:10,000, we can measure charges over a range of four decades, e.g., from 6×10^{-18} As to 6×10^{-14} As. Since the charge of a particle is proportional to its radius (equation 1), we can cover about four decades in particle radius or twelve decades in

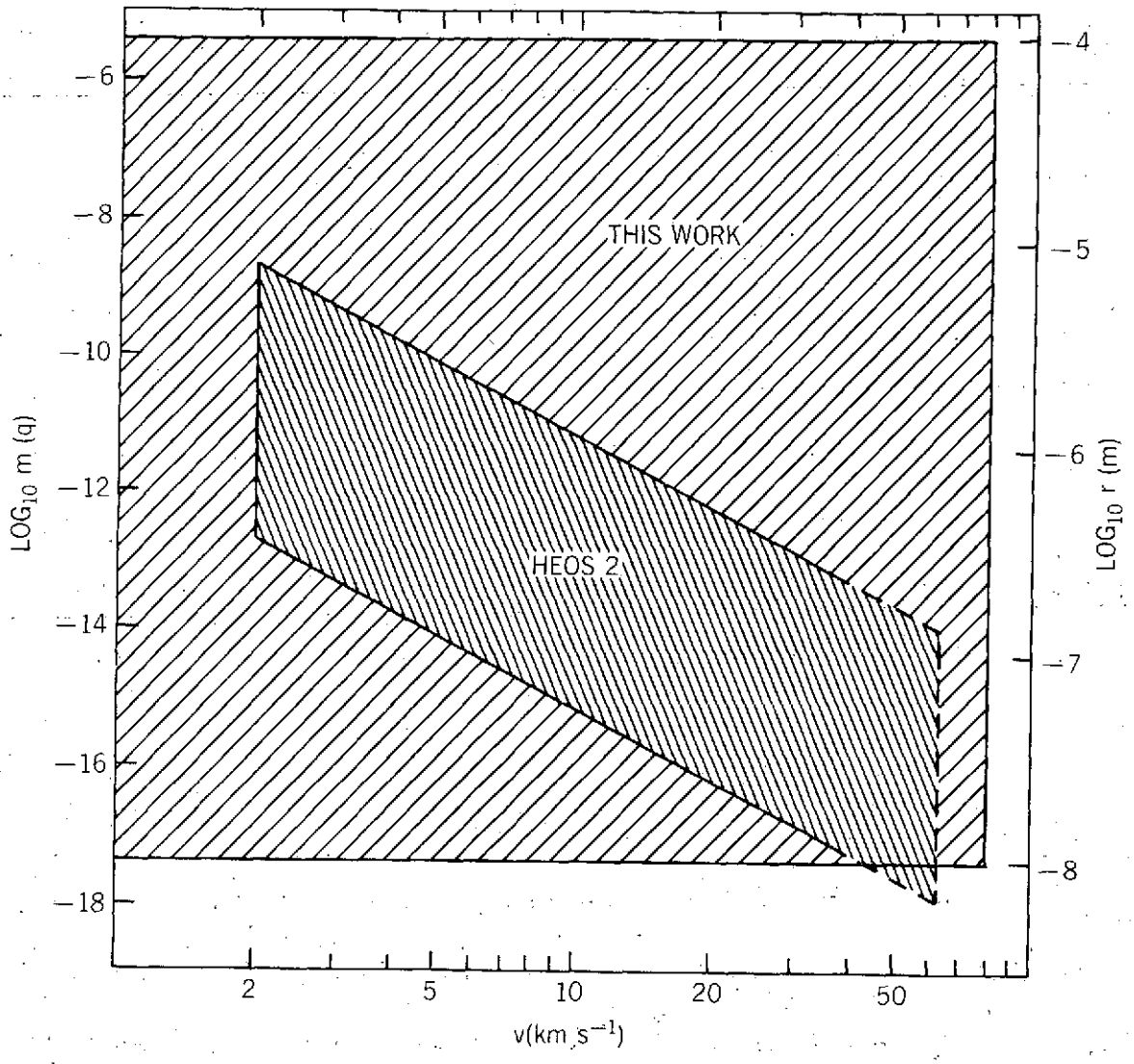

Figure 12. Comparison of the ranges of measurement of the HEOS 2 detector[9] and the techniques described in this paper. Particle mass m and radius r as a function of velocity v, assuming a density $\rho = 1\,\mathrm{g\,cm^{-3}}$.

particle mass. These ranges of sizes and velocities are much broader than any other single detector has covered before.

CONCLUSIONS

The ideal detector for cosmic dust particles should measure the velocity vector relative to the spacecraft, mass, charge, size, shape, and chemical composition

of each individual particle. This universal goal has been out of reach with prior techniques because at least one part of the measurement disturbed another part. We have come very close to this goal not only because the new methods provide the first precise measurement of the velocity vector, but also because the determination of orbital elements no longer disturbs a subsequent analysis of the particle composition. In addition, the new ranges of measurable particle sizes and velocities are considered to be so broad that virtually all possible cosmic dust particles fall within these ranges and no instrumental cutoff for some dust particles should exist any more. Data that can be obtained with these methods would certainly be of great value in the task of unravelling the complex problems of interplanetary and interstellar matter.

ACKNOWLEDGEMENTS

It is a pleasure to thank O. E. Berg for his continuous support and encouragement. H. Wolf of Analytical Mechanics Associates, Inc., performed the orbital calculation of model particles. The National Academy of Sciences provided the author with a senior resident research associateship.

REFERENCES

1. O. E. Berg and U. Gerloff, J. Geophys. Res. 75, 6932 (1970)
2. O. E. Berg, F. F. Richardson, and H. Burton, "Lunar Ejecta and Meteorites Experiment" in: Apollo 17: Preliminary Science Report, NASA SP-330, pp. 16-1 - 16-9 (1973)
3. O. E. Berg and E. Grün, "Evidence of Hyperbolic Cosmic Dust Particles" in: Space Research XIII, 1047 (1973)
4. H. A. Zook and O. E. Berg, "A Source for Hyperbolic Cosmic Dust Particles," Planet. Space Sci. (1974) in print
5. C. L. Hemenway, D. S. Hallgren, and D. C. Schmalberger, Nature 238, 256 (1972)
6. S. O. Auer, "Cosmic Dust or Other Similar Outer Space Particles Impact Location Detector," U.S. patent no. 3,694,655, filed Dec. 1970
7. J. W. Rhee, in: The Zodiacal Light and the Interplanetary Medium, NASA SP-150, 291 (1967)
8. R. C. Jennison and J. A. M. McDonnell, Planet. Space Sci. 12, 627 (1964)
9. H. Dietzel, G. Eichhorn, H. Fechtig, E. Grün, H. J. Hoffmann, and J. Kissel, J. Physics E: Sci. Instr., 6, 209 (1973)
10. K. Kandiah, Nucl. Instr. Meth., 95, 289 (1971)
11. V. Radeka and H. W. Kraner, "Design Study of a Solid-State Non-Dispersive X-Ray Spectrometer for a HEAO Mission," a report prepared for NASA, Goddard Space Flight Center, under Contract No. S-50025A (1974)

12. D. E. Stilwell, R. M. Joyce, J. H. Trainor, H. D. White, Jr., G. Streeter, and J. Bernstein, "The Pioneer 10/11 and Helios A/B Cosmic Ray Instruments," IEEE Trans. Nucl. Sci., NS22, in preparation (1975)

13. O. E. Berg, private communication (1973)

14. S. Auer and K. Sitte, Earth Plan. Sci. L. 4, 178 (1968)

15. J. F. Friichtenicht, N. L. Roy, and D. G. Becker, in: Evolutionary and Physical Properties of Meteoroids, NASA SP-319, 299 (1973)

16. S. O. Auer, "Micrometeoroid Analyzer," U.S. Patent No. 3,715,590, filed March 1971

17. S. O. Auer, "Moving Particle Composition Analyzer," patent pending, NASA case GSC 11, 889-1, Jan. 1974

18. S. F. Singer, in: Scientific Uses of Earth Satellites, Univ. of Michigan press, Ann Arbor, 301 (1956)

19. L. G. Jacchia, in: The Moon, Meteorites and Comets, Univ. of Chicago Press, Chicago, 774 (1963)

20. E. N. Parker, Astroph. J. 139, 951 (1964)

21 I. I. Shapiro, D. A. Lautman, and G. Colombo, a paper presented at the Symposium on Meteor Orbits and Dust, Aug. 9-13, 1965, Cambridge

22. T. Schmidt and H. Elsässer, in: The Zodiacal Light and the Interplanetary Medium, NASA SP-150, 287 (1967)

23. S. F. Singer, J. Geophys. Res. 67, 3599 (1962)

24. S. J. Peale, J. Geophys. Res. 71, 911 (1966)

25. A. D. Whalen, Detection of Signals in Noise, Academic Press, New York (1971)

26. Handbook of Tables for Probability and Statistics, ed. W. H. Beyer, The Chemical Rubber Co., Cleveland, Ohio (1968)